The 10th IEEE International Conference on Intelligent Data Acquisition and Advanced Computing Systems: Technology and Applications
18-21 September, 2019, Metz, France

Comparison of Pixel Correlation Induced by Space-Filling Curves on 2D Image Data

Stéphane Duguay[1], Steven Pigeon[2]
Université du Québec à Rimouski
300 Allée des Ursulines, Rimouski QC, G5L 3A1, Canada
[1] stephane.duguay@uqar.ca
[2] steven_pigeon@uqar.ca

***Abstract* — Space-filling curves are well known for preserving pixel locality when they are used as paths to traverse 2D image data. Some prediction-based compression algorithms make use of these curves to ensure high pixel values correlation during 2D image data traversal. This work explores the distribution of pixel correlation induced by all possible space-filling curves on 2D image data and demonstrates that commonly used curves, such as the Hilbert or the Peano curves, do not provide the best possible pixel correlation for natural photographic images. Using experimental data collected on a large set of such images, we demonstrate that row-prime ordering is the best choice for preserving maximum pixel values correlation while reducing the dimensionality of 2D natural photographic image data.**

Keywords* — *space-filling curves; pixel correlation; pixel locality; image compression; image processing

I. Introduction

Mapping 2D image data to a one-dimensional sequence of pixels is a common operation in image processing. A simple approach to reduce the dimensionality of pixel data is to concatenate, one after another, all the pixel rows (scanlines). In natural images, neighboring pixel values are usually highly correlated. With a simple concatenation, the resulting reordered pixels suffer pixel values discontinuity on scanline changes, which is not optimal for prediction-based compression algorithms that require high pixel correlation to achieve better compression ratios.

Space-filling curves (SFCs) [1] provide pixels traversal paths that preserve pixel locality, improving the correlation of pixel values over the scanlines concatenation approach. Some prediction-based compression algorithms [2]–[4] use well-known SFCs, such as Hilbert's [5] or Peano's [6], while other studies have optimized pixel values correlation using adaptive SFCs [7]–[13] but these adaptive approaches are data-dependent and require extra coding and storage.

This work investigates the distribution of pixel values correlation induced by data-independent SFCs, and which SFCs provide the best possible pixel values correlation for natural photographic image traversal.

II. Methodology

To quantify the pixel values correlation property of space-filling curves, we accumulated the error energy for each possible Hamiltonian paths on each pixel subsets (patches) of different sizes for 100 natural photographic images. Fig. 1 shows one of the images used in this work.

A. Images and Patches

To ensure that our results were color-component and resolution independent, each 24-bit image in the test set was processed at three different resolutions: 5202×3465 (original), 2601×1733 (half), and 1300×866 (quarter). Down-sampling was performed using ImageMagick's Blackman filter. The test set therefore comprises 300 images, for a total of 900 8-bit image planes.

In what follows, a patch is a $n\times n$ pixel region of an image, comprising all color planes. For this work, we considered patches of sizes 4×4 to 6×6. To not only generate a great number of patches but also, and maybe more importantly, to guard against alignment effects, all distinct $n\times n$ patches were extracted from an image, for a total of $(x-n+1)\times(y-n+1)$ patches for a $x\times y$ pixel image.

Figure 1: One of the natural photographic images used for this experiment (Seljalandsfoss, Iceland).

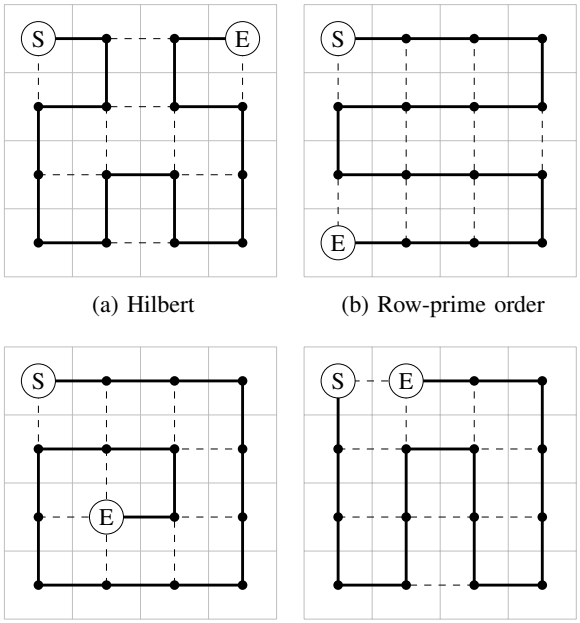

(a) Hilbert (b) Row-prime order

(c) Spiral (d) One of many others

Figure 2: Some 4×4 space-filling curves. Ⓢ indicates the starting pixel, and Ⓔ the ending pixel.

B. Hamiltonian Paths

A Hamiltonian path on a grid graph, or for our purpose, a *path*, is a path that visits every node exactly once. For our application, a node is a pixel, and the connectivity of the graph is limited by N-S-E-W neighbors within the $n\times n$ pixel patch. Fig. 2 shows examples of such paths.

While a number of previous studies limited themselves to a single path (either Hilbert or Peano) [2]–[4], or to a small number of preselected paths [7]–[10], or computed them in order to explicitly minimize a cost function [11]–[13], we intend to find the distribution of energy induced by *all* possible directed Hamiltonian paths in a $n\times n$ grid graph. Because the number of possible paths grows rapidly [14]–[16], we limited the experiment to grid graphs, or patches, of sizes 4×4 to 6×6.

C. Estimating Energy Induced by a Path

As an estimator of energy compaction under a wide variety of transforms [17], [18, Ch. 3], we used the sum of the squared difference between pixels along a path. The energy for a $n\times n$ single color component patch c unwound by path h is given by

$$\mathcal{E}(h,c) = \sum_{j=0}^{n^2-2} \left(c_{h_{j+1}} - c_{h_j}\right)^2 , \qquad (1)$$

where h_j is the coordinate of the j^{th} pixel along the path h. We accumulate the energy of every patch p of every color components c of every image i in the image test set I. The total energy over the test set is

$$\mathcal{E}(h,I) = \sum_{i\in I}\sum_{p\in i}\sum_{c\in p}\mathcal{E}(h,c) .$$

Size	Min	Hilbert	Max	Range
4×4	1.54×10^{12}	1.56×10^{12}	1.57×10^{12}	3.28×10^{10}
5×5	2.46×10^{12}	2.49×10^{12}	2.52×10^{12}	5.84×10^{10}
6×6	8.27×10^{12}	8.64×10^{12}	9.04×10^{12}	7.72×10^{11}

Table I: Total energies on full resolution images.

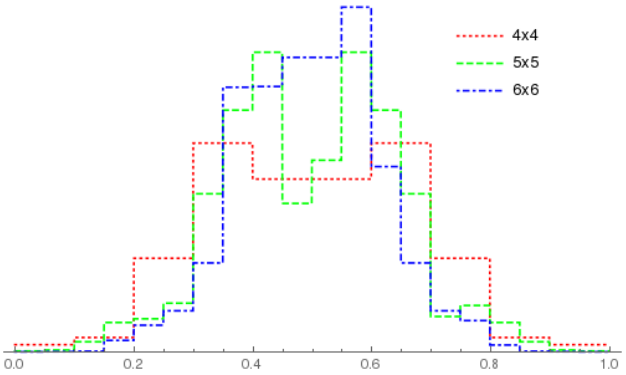

Figure 3: The distribution of energies induced by paths over 4×4 ■, 5×5 ■, and 6×6 ■ patches, on full resolution images.

III. Results

We estimated the energy induced by all SFCs on patches of sizes 4×4 to 6×6 over our 100 image test set at three different resolutions, resulting in the scan, for each path, of 900 8-bit image planes.

Fig. 3 shows the distribution of energy of all curves of sizes 4×4 to 6×6 over all the images in full resolution. The energies are normalized between zero and one, with zero corresponding to the lowest energy observed for a given experiment, and one to the highest. The histogram is then normalized in height so that the surface is one—a probability distribution. Figs. 4 and 5 show, respectively, the distributions of energy over all patches of sizes 4×4 and 5×5 over the three image resolutions, with the same normalization as fig. 3. We see that the distribution is very nearly resolution-independent, which is a desirable property, as it would indicate that the choice of path will not depend strongly on the resolution of the image. Figs. 6 and 7 show where the best and Hilbert curves are located relative to the distribution of energy. We see that the Hilbert curves perform very nearly like the average of curves. Since the Hilbert curve is well defined only for grid graphs of size $2^n\times2^n$ (with $n\geqslant2$), the curves retained for testing are necessarily different. Fig. 8 shows the Hilbert curves retained for comparison. The energies are summarized in table I.

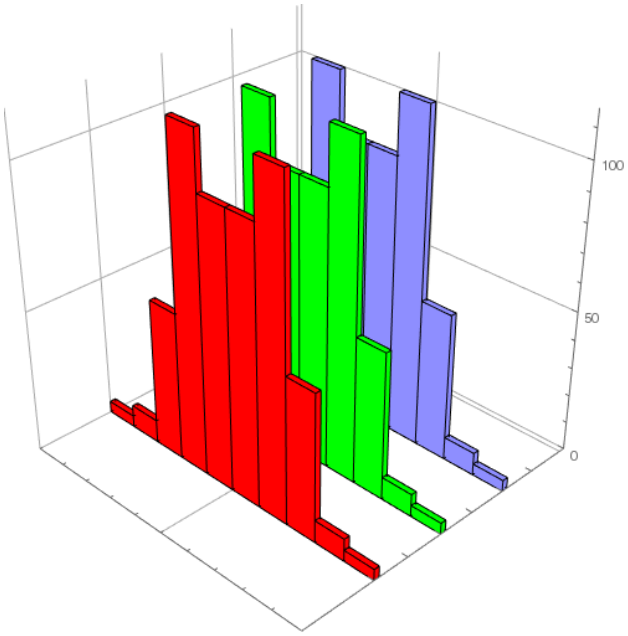

Figure 4: The distribution of energies induced by paths over 4×4 patches, from quarter ■, half ■, and full resolution ■ images.

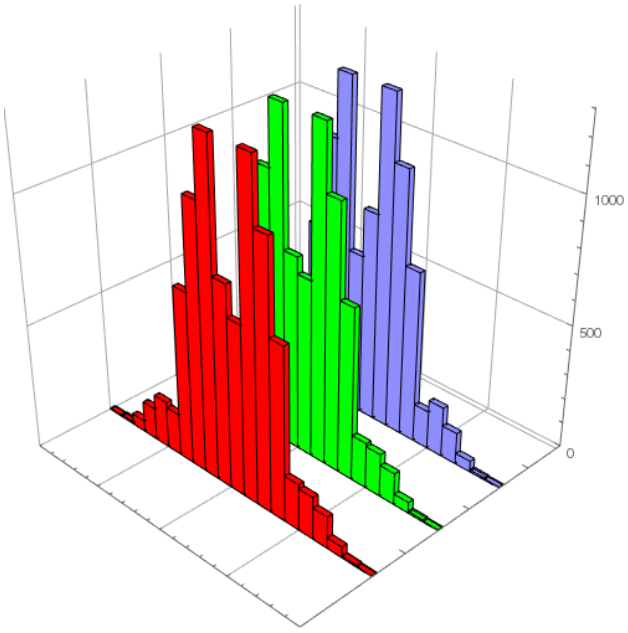

Figure 5: The distribution of energies induced by paths over 5×5 patches, from quarter ■, half ■, and full resolution ■ images.

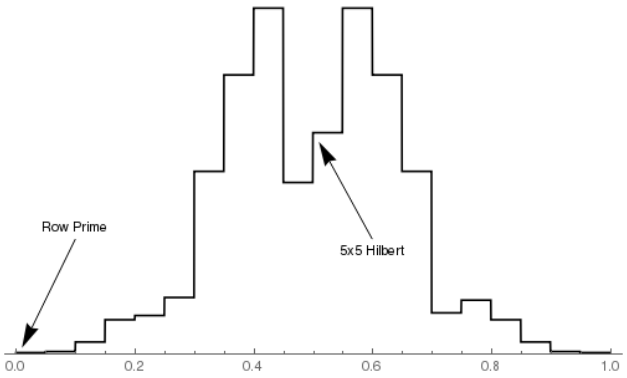

Figure 6: The location of various curves on 5×5 patches.

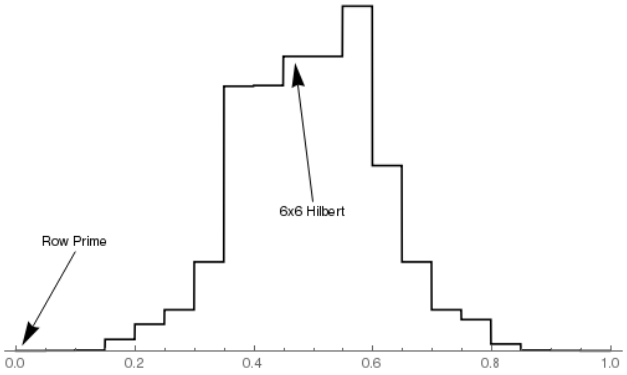

Figure 7: The location of various curves on 6×6 patches.

IV. Discussion

Figs. 6 and 7 show the relative energies induced by the selected curves. The best curve, row-prime ordering, is shown far left while the variants of Hilbert's curve (shown in fig. 8) are found near the center, indicating that Hilbert curves perform only like the average SFC in terms of induced energies. This is unexpected because the row-prime SFCs provide less pixel locality than popular SFCs such as the Hilbert curve or the even the Peano curve, but they do maximize correlation between pixels along their

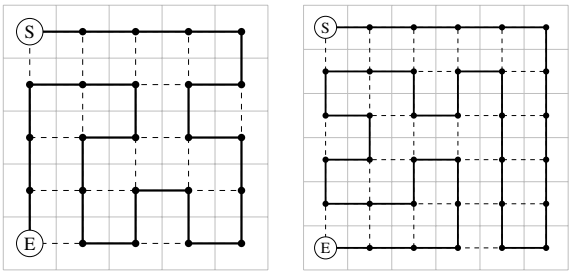

(a) 5×5 Hilbert. (b) 6×6 Hilbert.

Figure 8: Hilbert curves retained for figs. 6 and 7.

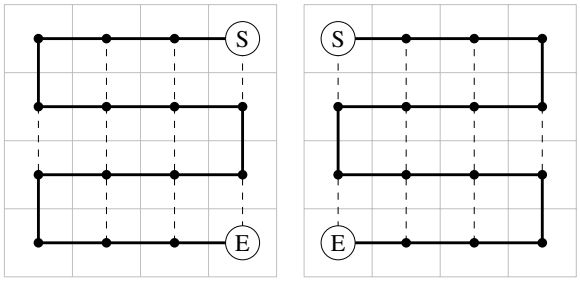

(a) Best (b) Second best

Figure 9: Best two paths at 4×4 patch size for all resolutions. Ⓢ indicates the starting pixel, and Ⓔ the ending pixel.

Data Set (count)	Average Energy Per Pixel Horiz.	Vert.	Relative Diff.
Kodak True Color (24)	23.62	26.06	9.36%
Our Data Set (100)	33.67	34.30	1.84%
Flickr Faces (70 000)	31.13	27.77	-10.79%
Open Images Ex (478 215)	122.78	124.34	1.25%

Table II: Comparison of average horizontal and vertical energies per pixel.

paths, at least as far as our extensive image test set is concerned.

One may also note that an effect of eq. (1) is that the energy is invariant in the direction of the path, and that, we essentially use undirected paths. Indeed, if we reverse the direction of the path, we compute the same squared differences along the way. Therefore, the selection of the best curves are up to a direction. However, we still need to differentiate orientation and mirroring (see fig. 9).

One may question if the effects observed are an artifact of the data set used. While we have yet to run the test with all the curves on larger data sets, we have measured that the vertical energy (column-prime) and horizontal energy (row-prime) shows approximately the same relative difference and preference to row-prime order. Table II shows the summary of these experiments. One notable difference is the Flickr Faces data set, which is exclusively composed of tightly-framed faces. There is otherwise no reason to think that our data set is different in any significant way.

Figs. 6 and 7, and also figs. 4 and 5, hint that energy is somewhat normally distributed if we consider all paths—we may even conjecture that as the patch size grows, the distribution will converge to a binomial distribution. That will be the object of further investigations.

V. Conclusion

While we may have the intuition that choosing a Hilbert-like SFC maximizing locality will also maximize correlation between successive pixels along its path, our experiment shows that it is not the case. Indeed, we have shown that row-prime (or column-prime in some cases) ordering gives better correlation on natural photographic images (such as fig. 1) than most other curves, and in particular, better than the Hilbert curve that performs only like the average of all possible curves for a given patch size. In spite of the appeal of regular and recursively defined SFCs such as the Hilbert or Peano curves, it may well be preferable to use a simpler, easier to implement, row-prime order curve, or one of its variations.

References

[1] H. Sagan, *Space-Filling Curves*. Springer Science & Business Media, 2012.

[2] J.-Y. Liang, C.-S. Chen, C.-H. Huang, and L. Liu, "Lossless compression of medical images using Hilbert space-filling curves," *Computerized Medical Imaging and Graphics*, vol. 32, no. 3, pp. 174–182, Apr. 2008.

[3] B. Moghaddam, K. J. Hintz, and C. V. Stewart, "Space-filling curves for image compression," F. A. Sadjadi, Ed., Orlando, FL, Aug. 1991, pp. 414–421.

[4] J. A. Provine, "Lossless compression of Peanoscanned images," *Journal of Electronic Imaging*, vol. 3, no. 2, p. 176, Apr. 1994.

[5] D. Hilbert, "Über die stetige Abbildung einer Linie auf ein Flächenstück," in *Dritter Band: Analysis· Grundlagen der Mathematik· Physik Verschiedenes*. Springer, 1935, pp. 1–2.

[6] G. Peano, "Sur une courbe, qui remplit toute une aire plane," *Mathematische Annalen*, vol. 36, no. 1, pp. 157–160, 1890.

[7] G. Drost and N. Bourbakis, "A hybrid system for real-time lossless image compression," *Microprocessors and Microsystems*, vol. 25, no. 1, pp. 19–31, Mar. 2001.

[8] R. Herrero and V. K. Ingle, "Space-filling curves applied to compression of ultraspectral images: Performance evaluation and analytical modeling," *Signal, Image and Video Processing*, vol. 9, no. 6, pp. 1249–1257, Sep. 2015.

[9] N. Memon, D. Neuhoff, and S. Shende, "An Analysis of Some Common Scanning Techniques for Lossless Image Compression," *IEEE Trans. Image Process.*, vol. 9, no. 11, pp. 1837–1848, 2000.

[10] T. Ouni and M. Abid, "Scan Methods and Their Application in Image Compression," *Image Processing and Pattern Recognition*, vol. 5, no. 3, p. 16, 2012.

[11] R. Dafner, D. Cohen-Or, and Y. Matias, "Context-based Space Filling Curves," *Computer Graphics Forum*, vol. 19, no. 3, pp. 209–218, Sep. 2000.

[12] S.-i. Kamata and Y. Hayashi, "Region-based scanning for image compression," in *Image Processing, 2000. Proceedings. 2000 International Conference on*, vol. 2. IEEE, 2000, pp. 895–898.

[13] T. Ouni, A. Lassoued, and M. Abid, "Gradient-based Space Filling Curves: Application to lossless image compression," in *2011 IEEE International Conference on Computer Applications and Industrial Electronics (ICCAIE)*. Penang, Malaysia: IEEE, Dec. 2011, pp. 437–442.

[14] J. L. Jacobsen, "Exact enumeration of hamiltonian circuits, walks and chains in two and three dimensions," *Journal of Physics A: Mathematical and Theoretical*, vol. 40, no. 49, pp. 14 667–14 678, nov 2007.

[15] J.-M. Mayer, C. Guez, and J. Dayantis, "Exact computer enumeration of the number of Hamiltonian Paths in small plane square lattices," *Physical Review B*, vol. 42, no. 1, pp. 660–664, Jul. 1990.

[16] J. W. Layman, "A096969: Number of ways to number the cells of an $n \times n$ square grid with 1,2,3,...,n^2 so that successive integers are in adjacent cells (horizontally or vertically)," Jul. 2004. [Online]. Available: http://oeis.org/A096969

[17] P. Yip and K. Rao, "Energy Packing Efficiency for the Generalized Discrete Transforms," *IEEE Trans. Commun.*, vol. 26, no. 4, pp. 1257–1262, 1978.

[18] V. Britanak, P. C. Yip, and K. R. Rao, *Discrete Cosine and Sine Transforms: General Properties, Fast Algorithms, and Integer Approximations*. Academic Press, 2006.